Kinematic Analysis of the Human Thumb with Foldable Palm

Visakha Nanayakkara[1], Ahmad Ataka[2], Demetrios Venetsanos[1], Olga Duran[1], Nikolaos Vitzilaios[1], Thrishantha Nanayakkara[2], and M. Necip Sahinkaya[1]

[1]School of Mechanical and Automotive Engineering,
Kingston University London, Kingston upon Thames, Surrey KT1 2EE, UK
{k1454696, D.Venetsanos, O.Duran, N.Vitzilaios, M.Sahinkaya}@kingston.ac.uk
[2] Department of Informatics, King's College London
{ahmad_ataka_awwalur.rizqi, thrish.antha}@kcl.ac.uk

Abstract. There have been numerous attempts to develop anthropomorphic robotic hands with varying levels of dexterous capabilities. However, these robotic hands often suffer from a lack of comprehensive understanding of the musculoskeletal behavior of the human thumb with integrated foldable palm. This paper proposes a novel kinematic model to analyze the importance of thumb-palm embodiment in grasping objects. The model is validated using human demonstrations for five precision grasp types across five human subjects. The model is used to find whether there are any co-activations among the thumb joint angles and muskuloskeletal parameters of the palm. In this paper we show that there are certain pairs of joints that show stronger linear relationships in the torque space than in joint angle space. These observations provide useful design guidelines to reduce control complexity in anthropomorphic robotic thumbs.

Keywords: Thumb kinematics, foldable palm, joint angle correlations, torque correlations

1 Introduction

It is a prerequisite to understand which attributes of the human hand are the most important to achieve functionality and agility for robotic hands that can be used in unstructured human environments. Though most features of the human hand have been studied and successfully replicated, the complex mechanism of how the thumb works together with the foldable palm is not well understood. Human motor capabilities are limited in kinematically-simplified hands [1]. However, there are many robotic hand applications in which simplified models are not sufficient since correct anatomical movement is a necessity such as in telemanipulation.

It is undoubted that the thumb plays a vital role in improving grasp performance and manipulation tasks. Human thumb has three joints, Carpometacarpal (CMC), Metacarpophalangeal (MCP), and Interphalangeal (IP). According to the studies in [2], a few postural synergies are sufficient to explain hand shape in pre-grasp, in which thumb adduction and internal rotation account for a considerable movement compared to that of MCP and IP.

There is less agreement about the kinematic thumb models that can be found in the literature. This is due to the different ways of defining thumb motion and the difficult nature of assigning classic planes to thumb movements and postures [3]. The proposed thumb kinematic description in [4], which has five Degrees of Freedom (DOF) along with a fixed carpal bone at the base of the thumb (trapezium), gives unrealistic torque/force values at the thumb tip. They suggest that abstracting bone architecture merely as invariant hinge type joints [5] does not represent the true transformation of muscle forces to thumb tip output. Authors in [6], [7] propose that including trapezium movement in thumb modeling and joint axes location movement could enhance accuracy. Since muscle forces affect thumb kinematics, a detailed kinematic description of the thumb is vital for robotic researchers and clinicians alike [4]. Thumb kinematics were studied *in vitro* based on axes of rotation of CMC, MCP, and IP joints in [8], [9]. According to them, abduction-adduction (A-A) axis of CMC is in the first metacarpal and flexion-extension (F-E) axis is in the trapezium. They suggest that the A-A and F-E motions that occur about these two non-orthogonal non-intersecting CMC axes, are not in the anatomic planes.

The number of DOFs required to fully describe the thumb mechanism and which DOFs are sufficient to grasp and manipulate objects designed for the human hand are contended. Even though IP joint was considered as 1-DOF in most of the kinematic thumb models [10], [11], MCP and CMC joints' DOFs were less agreed [8], [12], [5]. Active pronation-supination (P-S) movement at the CMC joint is 23^0 on average according to [12] indicating its significance in overall movement. Kinematic hand model developed in [7] for data glove calibration, used an unsensed axis along the metacarpal for P-S motion. According to [6], the widely accepted thumb kinematic model is the virtual five-link model presented in [5]. Moreover, the anatomical and functional characteristics of the human thumb can be modeled using the kinematic models in [13]. In any of these approaches, either trapezium is adopted as fixed or merely rigid bone rotations around joints are considered. Contribution of the foldable palm as a musculoskeletal structure is not considered in creating a kinematic model of the thumb.

In vivo studies in [14] indicate that muscles add more stability and passive guidance that merely a bone model cannot achieve. We introduce a 7-DOF thumb kinematic model with variable virtual link connections on the palm to analyze the role of thumb and foldable palm morphology in grasping. The model has 12 kinematic variables and parameters. It gives promising validation results using experimental data in thumb motion tracking for five subjects in precision grasping of five objects. It is a prerequisite to understand any available joint or link correlation patterns that contribute to reduce the complexity of these higher number of DOF (seven in this case). Therefore, we analyze any existing thumb joint angle and joint torque correlations using the proposed model that can be adopted in tendon transfer surgeries as well as in robotic hand design.

The rest of the paper is arranged in the following order. In section 2, the proposed kinematic model methodology is discussed in detail. Kinematic model validation results and joint angle/torque correlations are elaborated in sections 3. Section 4 provides discussion followed by the conclusion.

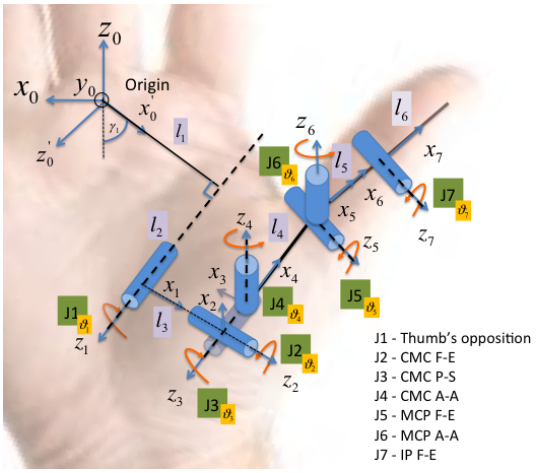

Fig. 1. 7-DOF thumb kinematic model. J1-J7 joint rotational movements are represented by $\theta_1 - \theta_7$. Thumb link lengths $l_5 - l_6$ are measured values from the subjects whereas $l_1 - l_4$ and γ_1 are model parameters.

Table 1. D-H parameters of the 7-DOF thumb kinematic model

Frame number	Link twist (deg.)	Link length (cm)	Link offset (cm)	Joint angle (deg.)
0	0	0	0	0
1	0	l_1	l_2	θ_1
2	90	0	l_3	θ_2
3	-90	0	0	θ_3
4	90	0	0	θ_4
5	90	l_4	0	θ_5
6	-90	0	0	θ_6
7	90	l_5	0	θ_7
8	0	l_6	0	0

2 Methodology

2.1 Kinematic Thumb Design

The proposed kinematic thumb model with integrated palm musculoskeletal behavior, has 7-DOFs (J1-J7) represented by revolute joints for each rotational movement (Fig. 1). In Fig. 1, coordinate frames for each joint, link connections and design parameters of the kinematic chain are defined according to the Denavit-Hartenberg (D-H) notation [15] (Table 1). The origin of the reference frame is taken to align with the human data reference, which is the CMC joint of the middle finger. The origin x and z axes, which lie on the palm plane, are rotated (90+γ_1) around y axis to align x axis along the link length l_1. The virtual link lengths $l_1 - l_4$ and γ_1 on $x - z$ space tend to vary due to the muscles and ligaments that act on the thumb.

Among seven muscles and the ligaments, that maintain the stability of the CMC joint, adductor pollicis (oblique head) muscle inserts the largest torque across the palm [16], [17]. We abstract this musculoskeletal behavior into the virtual joint, J1 to represent thumb's opposability with the foldable palm. J1's rotational axis lies along virtual link l_2, which is the foldabe palm crease. This joint provides interaction between thumb and the fingers allowing it to grasp various sizes and shapes. Virtual link lengths l_1, l_2, and l_3 are orthogonal in corresponding order.

Thumb's CMC joint is approximated into three revolute joints with orthogonal and intersecting rotational axes for F-E (J2), P-S (J3), and A-A (J4) with their intersecting point on the palm plane to kinematically analyze their individual contribution in CMC joint motion as a whole (in Fig. 1, these three joint axes are shown apart for clarity). P-S axis lies along link l_4 which is more or less the thumb's 1^{st} metacarpal [12]. Merely solid bone structure will not represent kinematics properly, unless the enveloping muscles' contribution in grasping is included [18]. Hence, link lengths $l_1 - l_4$ cannot be fixed when MCP-IP-thumb tip-linkage movement occurs in coordination with the CMC joint movement.

Authors in [8] prove that MCP joint has A-A and F-E axes and the angle between them is $85^0 \pm 12^0$. We approximate 2-DOF MCP joint (J5-J6) A-A axis as orthogonal to F-E axis and IP joint (J7) has only single DOF (F-E). F-E axes of MCP and IP are taken to be parallel to each other and align along the biological joint axes.

Relative joint angle ranges and rotation directions of the revolute joints are determined based on the D-H convention [15]. Parameter/variable boundaries and initial values are tuned using forward kinematics that produce anatomically feasible motions as possible.

Each consecutive joint position and orientation (Fig. 1) can be evaluated using link parameters assigned in Table 1 and transforming frame N corresponding to the N^{th} joint to reference frame 0 using the transformation,

$$ {}^{0}_{N}T = \prod_{i=0}^{N-1} {}^{i}_{i+1}T \tag{1} $$

where the matrices ${}^{i}_{i+1}T, i = 0, 1, 2, \cdots, 8$ are shown in the Appendix. Taking the product of N transforms for each joint gives the standard homogeneous transformation matrix for the N^{th} joint relative to the reference frame [15]. Since N depends on the configuration of the model, $N = 7$ gives the standard homogeneous transformation matrix for the MCP joint with respect to the reference and $N = 9$ gives that of the tip. These kinematic model position values are compared against human thumb grasp data for the MCP joint and thumb tip for validation.

2.2 Human Grasp Data Acquisition

The NDI Aurora electromagnetic tracking system is used to capture the thumb motion using three magnetic sensors. The 6-DOF sensors are placed on the dorsal side of the prominent hand's thumb fingernail, thumb MCP joint and one as the reference on the MCP of the middle finger as shown in Fig. 2. We measure thumb tip and MCP joint movement since these two locations are the most identifiable kinematic landmarks. The

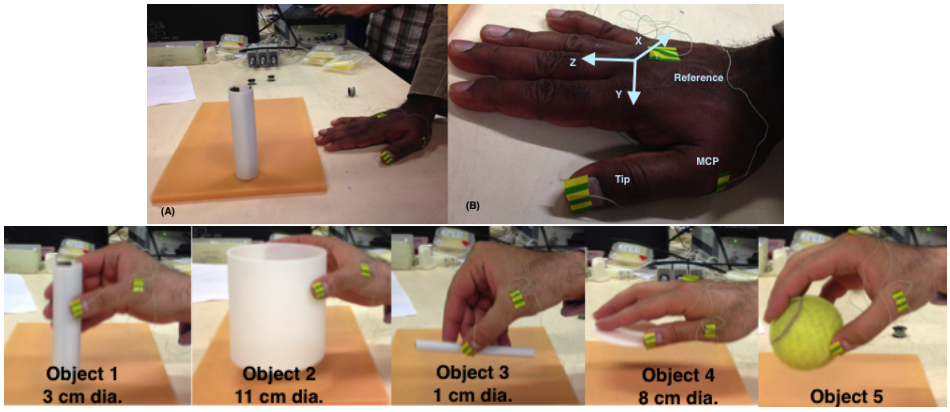

Fig. 2. (*top-A*) Initial experimental setting, (*top-B*) Sensor positions on the hand, (*bottom*) Grasping objects 1-5 for data collection.

position and orientation of each sensor is measured with respect to the reference sensor. The measurement rate is 40 Hz and the sensor accuracy is 0.48 mm for position and 0.30^0 for orientation inside the (0.5x0.5x0.5) m cube volume region next to the field generator. Three male and two female subjects participate in grasping five objects (Fig. 2). Object dimensions and reference sensor positions (Fig. 2) are adopted from [19]. Each subject is instructed to move the flat hand from the start position, grasp the object in precision grasp strategy without squeezing the object as much as possible, lift it, place it in a new marked position (25 cm apart) and move the hand back to the original position (Fig. 2). Each grasp type is done four times for each object. Data recording is started when the hand moves from the starting position and finished when it comes back to the initial position.

2.3 Kinematic Model Variable and Parameter Estimation

The MATLAB Global Optimization Toolbox is utilized to optimize the 12 parameters of the inverse kinematic model in Fig. 1. Since the error at the thumb tip is contributed by seven DOFs and that at the MCP is contributed by only four DOFs, we introduce two cost functions: C_1 and C_2 (**Algorithm 1**). Then solutions for C_1 and C_2 are obtained using a multi-objective optimization Genetic Algorithm (MATLAB function *gamultiobj*) [20] with population size 100 and maximum number of generations 150. The cost functions were introduced in two steps following [21], [22].

Let $P_h = [H_x \;\; H_y \;\; H_z]$ and $P_r = [R_x \;\; R_y \;\; R_z]$ denote the position vector of each human data point and that of the kinematic model respectively. Then the Euclidean distance of the two position vectors is given by,

$$E_p = \left[(P_h - P_r)^T (P_h - P_r)\right]^{1/2} \tag{2}$$

where C_1 and C_2 in **Algorithm 1** denote E_p at MCP joint and thumb tip positions respectively.

Data: Human grasp data (for MCP joint and thumb tip) and thumb kinematics
Result: Optimum joint movements
Initialize joint angles to $\theta_{0,1-4}$, link inclination to γ_0 and link lengths to l_0 ;
while $C_1 >$ *threshold A* **do**
  Run Matlab θ_{1-4}, γ_1, l_{1-4} = gamultiobj(E_p, $\theta_{0,1-4}$, γ_0, l_0);
  if $C_1 <$ *threshold B* **then**
    Exit with the optimum joint angles, θ^*_{1-4}, link inclination, γ^*_1 and link lengths, l^*;
  else
    Loop again;
  end
end
Initialize joint angles to optimized θ^*_{1-4}, initialize other joint angles, $\theta_{0,5-7}$, link inclination, γ^*_1 and link lengths, l^*;
while C_1, $C_2 >$ *threshold C* **do**
  Run Matlab θ_{1-7}, γ_1, l_{1-4} = gamultiobj(E_p, θ^*_{1-4}, $\theta_{0,5-7}$,γ_0, l_0);
  if C_1, $C_2 <$ *threshold D* **then**
    Exit with the optimum joint angles, θ^*_{1-7}, link inclination, γ^*_1 and link lengths, l^*;
  else
    Loop again;
  end
end

Algorithm 1: Finds optimum kinematic model joint parameters/variables for both MCP and thumb tip human trajectories. C_1: Euclidean error at the MCP joint, C_2: Euclidean error at the thumb tip. θ and l are the angles and links vectors respectively.

2.4 Joint Angle and Emulated Torque Correlations

In order to identify strong correlations between pairs of joint angles and joint torques in the kinematic model, we look at the R^2 values of linear regression during the pre-grasp and grasp stages. The R^2 value represents the degree to which the model explains the variability of the two variables considered in any given pair. Therefore relatively high R^2 values indicate that there is a high linear relationship between the pair of variables concerned than the others. In all the trials, 100 data points are used from the transient period so that 90 data samples are before and 10 data samples after the point at which the thumb tip touches the object.

Moreover, joint torques due to thumb tip-object interaction forces are examined to see whether there are any correlated joint torques which facilitate precision grasping. Equation (3) is used to calculate joint torques τ for 0.5^0 increments in all joints for an isometric 3D virtual unit vector force F (in N) at the thumb tip.

$$\tau = J^T F \tag{3}$$

where τ is the 7×1 torque vector, J is the 3×7 Jacobian matrix, and F is the 3×1 unit vector force.

These calculations are based on subject-wise virtual palm and real thumb link lengths (measured in cm). The virtual force vector applied in the overall transient thumb trajectory consists of 100 data points. To make it fair for all the trials, the transient period is evaluated 50 data points in either direction from the point where thumb tip touches

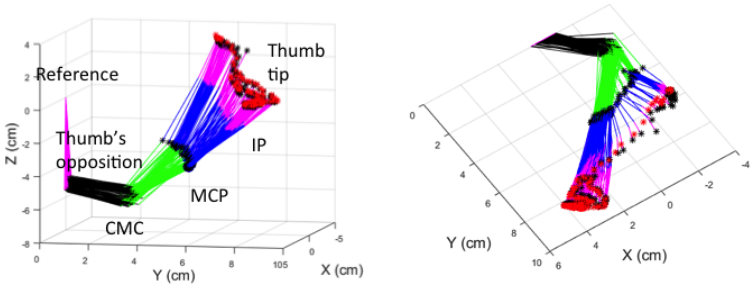

Fig. 3. Human thumb MCP joint and tip trajectories for a selected grasp type (tennis ball) with the corresponding fitted thumb kinematic model. Each link is drawn in a different color. (*left*) Overall trajectory in $x-y-z$ space, (*right*) rotated version of the same trajectory in $x-y$ space.

the object. This approach shows how the thumb prepares to take the force and how it apportions the torque τ among the joint configuration once the contact is established with the object.

3 Results

3.1 Kinematic Model Validation

The validated kinematic model gives Root Mean Square Error (RMSE) for MCP position < 0.5 cm and that for thumb tip position < 0.9 cm across all the five subjects, four trials and five grasp types. Fig. 3 illustrates a representative kinematic model fit with joint and link variations in overall thumb trajectory in grasping object 2 (11 cm dia. cylinder) with experimental data in $x-y-z$ space (defined in Fig. 1). The figure indicates the individual joint Range of Motion (ROM) at the foldable palm, CMC, MCP and IP joints. Each kinematic linkage of this trajectory is caused by 12 kinematic model variables and parameters. Corresponding thumb MCP and tip movements in x, y, and z space for four trials are shown in Fig. 4.

3.2 Joint Angle and Torque Correlations

According to joint angle correlation analysis using optimized thumb joint rotations ($\theta_1 - \theta_7$) during pre-grasp and grasp stage, we can observe that $R^2 > 0.8$ in joint pair number 20 (θ_5 and θ_7) associated with MCP and IP joint flexions in Fig. 5 (blue plots).

In torque correlations (red plots), joint pair number 8 (τ_2 and τ_4 represented by CMC flexion and abduction) also show $R^2 > 0.8$ along with number 20 (τ_5 and τ_7). These two highly correlated torque pairs are plotted in Fig. 6 across subjects, objects and trials. It shows higher torque values in the proximal pair (associated with CMC abduction and flexion) than the distal pair (MP and IP flexion).

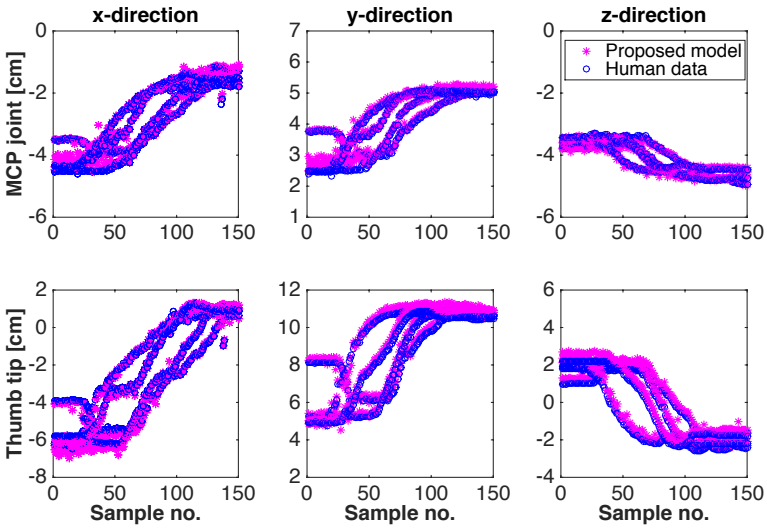

Fig. 4. A representative thumb MCP joint and tip trajectories (human and kinematic) in $x-y-z$ space plotted against the sample number.

4 Discussion

Experimental validation of the proposed kinematic model based on thumb and integrated foldable palm gives promising results with RMSE for MCP position < 0.5 cm and that for thumb tip position < 0.9 cm across all the five subjects, four trials and five grasp types. Authors in [4] point out the lack of experimentally validated thumb kinematic descriptions and the absence of inter-subject variability in so far adopted models. Since the proposed kinematic model incorporates inter-subject differences in palm musculostructure with variable links, it can be adopted in calculating inter-subject grip forces and torques.

We observe $R^2 > 0.8$ for thumb MCP and IP joint flexion pair in both pre-grasping and grasping the objects. According to [23], ROM among thumb joint angles is different due to enveloping muscle and ligament structure constraints. Angular ROMs of CMC and MCP joints during functional motion are less than 65% of their maximum ranges [24]. In [25], CMC and MCP A-A motions are correlated only during initial stage of thumb's opposition motion and not in the whole trajectory. Based on these findings, each thumb joint shows limited movement depending on the tasks. This behaviour could be the reason why we cannot find any other strong joint angle correlations in thumb joints while grasping.

The two rigid link thumb models adopted in [26] to compare tendon tension in thumb joints show that CMC joint flexion and abduction muscle relationships are poorly estimated. They point out the non-independent modeling of CMC P-S could be one factor. Whereas in our results, torque associated with CMC flexion and abduction axes shows strong correlation. According to the biomechanical studies in [14], Opponens

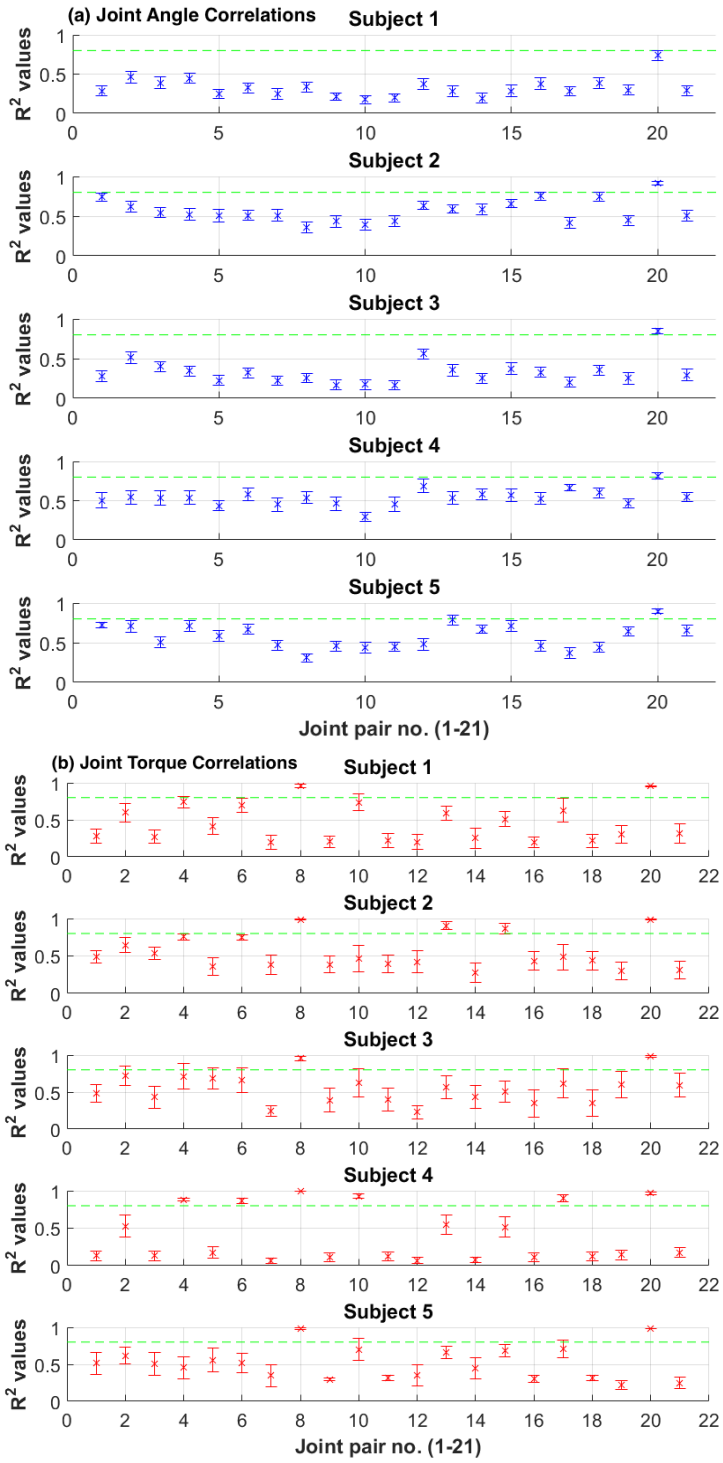

Fig. 5. R^2 values for (a) joint angle and (b) joint torque correlations plotted against 21 pairs of 7-joints for five subjects. The vertical error bars represent the standard error across five objects and four trials. Green lines mark $R^2 = 0.8$. The order of joint pairs (1-21) are given in Table 2.

Table 2. Joint pair numbers

Joint pair no.	Joint angles	Joint pair no.	Joint angles	Joint pair no.	Joint angles
1	θ_1, θ_2	8	θ_2, θ_4	15	θ_3, θ_7
2	θ_1, θ_3	9	θ_2, θ_5	16	θ_4, θ_5
3	θ_1, θ_4	10	θ_2, θ_6	17	θ_4, θ_6
4	θ_1, θ_5	11	θ_2, θ_7	18	θ_4, θ_7
5	θ_1, θ_6	12	θ_3, θ_4	19	θ_5, θ_6
6	θ_1, θ_7	13	θ_3, θ_5	20	θ_5, θ_7
7	θ_2, θ_3	14	θ_3, θ_6	21	θ_6, θ_7

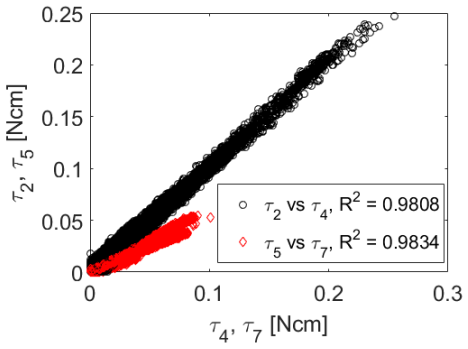

Fig. 6. Linearly correlated joint torque pairs with $R^2 > 0.8$.

Pollicis (OPP) muscle activity contributes 80% for flexion and 100% for abduction at CMC joint. Our results (Fig. 5) are consistent with them showing a strong joint torque correlation ($R^2 = 0.9808$) in CMC flexion and abduction for precision grasping. This reliable prediction could come from the following factors considered in the kinematic model: 1) CMC joint is modeled as three separate DOFs. Hence P-S is a kinematically independent motion within CMC. 2) A virtual joint J1 (Fig. 1) is introduced to abstract thumb's opposition. (Relatively higher torque correlation can be observed in joint axes pair J1 and CMC P-S than that of joint axes pair J1 and CMC F-E.) 3) Subject-wise link length variations are accounted.

However, the authors in [27] point out that CMC and MCP A-A are correlated. Our results do not illustrate this behaviour. It could also be due to the model CMC A-A and MCP A-A axes lie on the same $y-z$ plane. In addition, MCP flexion could be the dominant motion compared to abduction in precision grasping.

5 Conclusion

The proposed novel kinematic model for the thumb and the foldable palm explains the essential musculoskeletal behaviors in grasping. The model shows a strong joint angle correlation in MCP and IP flexion while having strong torque relationships in CMC

abduction and flexion pair and MP and IP flexion pair. The proposed modeling approach provides a model to determine tendon routing and pulling forces in anthropomorphic robotic thumbs.

References

1. Martell, J.S., Gini, G.: Robotic hands: Design review and proposal of new design process. World Academy of Science, Engineering and Technology **26** (2007) 85–90
2. Santello, M., Flanders, M., Soechting, J.F.: Postural hand synergies for tool use. The Journal of Neuroscience **18**(23) (1998) 10105–10115
3. Grinyagin, I.V., Biryukova, E.V., Maier, M.A.: Kinematic and dynamic synergies of human precision-grip movements. Journal of Neurophysiology **94**(4) (2005) 2284–2294
4. Valero-Cuevas, F.J., Johanson, M.E., Towles, J.D.: Towards a realistic biomechanical model of the thumb: the choice of kinematic description may be more critical than the solution method or the variability/uncertainty of musculoskeletal parameters. Journal of Biomechanics **36**(7) (2003) 1019–1030
5. Giurintano, D., Hollister, A., Buford, W., Thompson, D., Myers, L.: A virtual five-link model of the thumb. Medical Engineering & Physics **17**(4) (1995) 297–303
6. Bullock, I.M., Borràs, J., Dollar, A.M.: Assessing assumptions in kinematic hand models: a review. In: 4th IEEE RAS & EMBS International Conference on Biomedical Robotics and Biomechatronics (BioRob). (2012) 139–146
7. Griffin, W.B., Findley, R.P., Turner, M.L., Cutkosky, M.R.: Calibration and mapping of a human hand for dexterous telemanipulation. In: ASME IMECE 2000 Symposium on Haptic Interfaces for Virtual Environments and Teleoperator Systems. (2000) 1–8
8. Hollister, A., Giurintano, D.J., Buford, W.L., Myers, L.M., Novick, A.: The axes of rotation of the thumb interphalangeal and metacarpophalangeal joints. Clinical Orthopaedics and Related Research **320** (1995) 188–193
9. Hollister, A., Buford, W.L., Myers, L.M., Giurintano, D.J., Novick, A.: The axes of rotation of the thumb carpometacarpal joint. Journal of Orthopaedic Research **10**(3) (1992) 454–460
10. Chang, L.Y., Matsuoka, Y.: A kinematic thumb model for the act hand. In: IEEE International Conference on Robotics and Automation (ICRA), IEEE (2006) 1000–1005
11. Chalon, M., Grebenstein, M., Wimböck, T., Hirzinger, G.: The thumb: guidelines for a robotic design. In: IEEE/RSJ International Conference on Intelligent Robots and Systems (IROS). (2010) 5886–5893
12. Chang, L.Y., Pollard, N.S.: Method for determining kinematic parameters of the in vivo thumb carpometacarpal joint. IEEE Transactions on Biomedical Engineering **55**(7) (2008) 1897–1906
13. Santos, V.J., Valero-Cuevas, F.J.: Reported anatomical variability naturally leads to multimodal distributions of Denavit-Hartenberg parameters for the human thumb. IEEE Transactions on Biomedical Engineering **53**(2) (2006) 155–163
14. Kaufman, K.R., An, K.N., Litchy, W.J., Cooney, W.P., Chao, E.Y.: In-vivo function of the thumb muscles. Clinical Biomechanics **14**(2) (1999) 141–150
15. Craig, J.J.: Introduction to robotics: mechanics and control. Volume 3. Upper Saddle River: Pearson Prentice Hall (2005)
16. Smutz, W.P., Kongsayreepong, A., Hughes, R.E., Niebur, G., Cooney, W.P., An, K.N.: Mechanical advantage of the thumb muscles. Journal of Biomechanics **31**(6) (1998) 565–570
17. Neumann, D.A., Bielefeld, T.: The carpometacarpal joint of the thumb: stability, deformity, and therapeutic intervention. Journal of Orthopaedic & Sports Physical Therapy **33**(7) (2003) 386–399

18. Ladd, A.L., Crisco, J.J., Hagert, E., Rose, J., Weiss, A.P.C.: The 2014 abjs nicolas andry award: The puzzle of the thumb: Mobility, stability, and demands in opposition. Clinical Orthopaedics and Related Research® **472**(12) (2014) 3605–3622
19. Feix, T., Romero, J., Ek, C.H., Schmiedmayer, H.B., Kragic, D.: A metric for comparing the anthropomorphic motion capability of artificial hands. IEEE Transactions on Robotics **29**(1) (2013) 82–93
20. Deb, K.: Multi-objective optimization using evolutionary algorithms. Volume 16. John Wiley & Sons (2001)
21. Nanayakkara, T., Watanabe, K., Kiguchi, K., Izumi, K.: Evolving a multiobjective obstacle avoidance skill of a seven-link manipulator subject to constraints. International Journal of Systems Science **35**(3) (2004) 167–178
22. Nanayakkara, T., Kiguchi, K., Murakami, T., Watanabe, K., Izumi, K.: Skillful adaptation of a 7-dof manipulator to avoid moving obstacles in a teleoperated force control task. In: IEEE International Symposium on Industrial Electronics (ISIE). Volume 3. (2001) 1982–1987
23. Cooney, W.P., Lucca, M.J., Chao, E., Linscheid, R.: The kinesiology of the thumb trapeziometacarpal joint. The Journal of Bone & Joint Surgery **63**(9) (1981) 1371–1381
24. Tang, J., Zhang, X., Li, Z.M.: Operational and maximal workspace of the thumb. Ergonomics **51**(7) (2008) 1109–1118
25. Li, Z.M., Tang, J.: Coordination of thumb joints during opposition. Journal of biomechanics **40**(3) (2007) 502–510
26. Vigouroux, L., Domalain, M., Berton, E.: Comparison of tendon tensions estimated from two biomechanical models of the thumb. Journal of Biomechanics **42**(11) (2009) 1772–1777
27. Hollister, A., Giurintano, D.J.: Thumb movements, motions, and moments. Journal of Hand Therapy **8**(2) (1995) 106–114

6 APPENDIX: The transformation matrices for the kinematic model

$$ {}^{0}_{1}T = \begin{bmatrix} cos(90+\gamma_1) & 0 & sin(90+\gamma_1) & 0 \\ 0 & 1 & 0 & 0 \\ -sin(90+\gamma_1) & 0 & cos(90+\gamma_1) & 0 \\ 0 & 0 & 0 & 1 \end{bmatrix} \quad {}^{1}_{2}T = \begin{bmatrix} cos(\theta_1) & -sin(\theta_1) & 0 & l_1 \\ sin(\theta_1) & cos(\theta_1) & 0 & 0 \\ 0 & 0 & 1 & l_2 \\ 0 & 0 & 0 & 1 \end{bmatrix} $$

$$ {}^{2}_{3}T = \begin{bmatrix} cos(\theta_2) & -sin(\theta_2) & 0 & 0 \\ 0 & 0 & -1 & -l_3 \\ sin(\theta_2) & cos(\theta_2) & 0 & 0 \\ 0 & 0 & 0 & 1 \end{bmatrix} \quad {}^{3}_{4}T = \begin{bmatrix} cos(\theta_3) & -sin(\theta_3) & 0 & 0 \\ 0 & 0 & 1 & 0 \\ -sin(\theta_3) & -cos(\theta_3) & 0 & 0 \\ 0 & 0 & 0 & 1 \end{bmatrix} $$

$$ {}^{4}_{5}T = \begin{bmatrix} cos(\theta_4) & -sin(\theta_4) & 0 & 0 \\ 0 & 0 & -1 & 0 \\ sin(\theta_4) & cos(\theta_4) & 0 & 0 \\ 0 & 0 & 0 & 1 \end{bmatrix} \quad {}^{5}_{6}T = \begin{bmatrix} cos(\theta_5) & -sin(\theta_5) & 0 & l_4 \\ 0 & 0 & -1 & 0 \\ sin(\theta_5) & cos(\theta_5) & 0 & 0 \\ 0 & 0 & 0 & 1 \end{bmatrix} $$

$$ {}^{6}_{7}T = \begin{bmatrix} cos(\theta_6) & -sin(\theta_6) & 0 & 0 \\ 0 & 0 & 1 & 0 \\ -sin(\theta_6) & -cos(\theta_6) & 0 & 0 \\ 0 & 0 & 0 & 1 \end{bmatrix} \quad {}^{7}_{8}T = \begin{bmatrix} cos(\theta_7) & -sin(\theta_7) & 0 & l_5 \\ 0 & 0 & -1 & 0 \\ sin(\theta_7) & cos(\theta_7) & 0 & 0 \\ 0 & 0 & 0 & 1 \end{bmatrix} \quad {}^{8}_{9}T = \begin{bmatrix} 1 & 0 & 0 & l_6 \\ 0 & 1 & 0 & 0 \\ 0 & 0 & 1 & 0 \\ 0 & 0 & 0 & 1 \end{bmatrix} $$